EXOSKELETON

Estimating human joint moments unifies exoskeleton control, reducing user effort

Dean D. Molinaro[1,2]*, Inseung Kang[3], Aaron J. Young[1,2]

Robotic lower-limb exoskeletons can augment human mobility, but current systems require extensive, context-specific considerations, limiting their real-world viability. Here, we present a unified exoskeleton control framework that autonomously adapts assistance on the basis of instantaneous user joint moment estimates from a temporal convolutional network (TCN). When deployed on our hip exoskeleton, the TCN achieved an average root mean square error of 0.142 newton-meters per kilogram across 35 ambulatory conditions without any user-specific calibration. Further, the unified controller significantly reduced user metabolic cost and lower-limb positive work during level-ground and incline walking compared with walking without wearing the exoskeleton. This advancement bridges the gap between in-lab exoskeleton technology and real-world human ambulation, making exoskeleton control technology viable for a broad community.

INTRODUCTION

Realizing lower-limb exoskeleton technology in the real world would enable human mobility to reach new feats, making heavy boxes feel lighter in the warehouse (*1*), increasing the success rate of search and rescue operations (*2*), or even enabling new innovations in athletic training and exercise. To date, lower-limb exoskeletons have had substantial success in improving human mobility, including augmenting human energetics by offloading or adding to the mechanical work done by the underlying human musculature (*3*–*9*). Although the tangible benefits and potential societal effects of these devices continue to be found, we fail to see this technology deployed in the real world. So, the question remains, what is preventing exoskeleton technology from being realized "in the wild"?

One critical challenge lies within the exoskeleton controller (*3*, *4*, *10*, *11*). Generally, exoskeleton controllers are divided into three layers: high-level, mid-level, and low-level (*12*). The high-level layer estimates user and environmental states, such as ambulation mode (*9*, *13*–*17*) or ground slope (*18*, *19*), used to modulate assistance with changes in user joint demands. The state estimates are passed to the mid-level layer, which computes desired assistance on the basis of predefined control laws, such as spline-based assistance trajectories (*8*, *20*, *21*). The low-level layer then converts the desired exoskeleton assistance into actuator commands, often using motor-level state feedback control. Although human-in-the-loop optimization (*8*, *20*–*22*) and on-the-fly metabolic cost estimation (*23*, *24*) can optimize and personalize assistance, these methods require reoptimizing controller gains for each high-level state, an inherently time-intensive process. Further, these advances in mid-level control are dependent on accurate high-level state estimates. Although physics-driven (*9*, *17*, *25*) and data-driven (*13*–*16*, *18*, *19*, *26*–*28*) models can estimate one or more high-level states, defining, estimating, and subsequently optimizing high-level and mid-level controllers for all of the possible states needed to parameterize human movement in-the-wild is intractable.

Instead, instantaneous estimates of the user's underlying joint moments could replace conventional high-level states (*29*–*39*). Because lower-limb joint moments naturally vary across ambulation modes and conditions (*40*), lower-limb joint moments could serve as a single, continuous high-level state for modulating exoskeleton assistance. However, human joint moments cannot be directly measured but are instead computed post hoc using high-fidelity motion capture and six-axis force plate measurements from stationary in-lab equipment (*41*). Replacing these in-lab systems with current wearable sensor technology results in incomplete information, such as missing ground shear forces (*42*), and requires potentially cumbersome kinematic sensing of the distal joints along the limb. These limitations hinder the viability of analytical inverse dynamics solutions from wearable sensors alone, especially for more proximal joints.

Recent advances in data-driven approaches have improved the mapping between wearable sensor data and user joint moments, even with little to no user-specific data (*29*–*31*, *34*–*39*). Using these methods, researchers have conducted initial experiments using instantaneous joint moment estimates in the exoskeleton control loop (*29*–*31*, *37*–*39*). For instance, Gasparri *et al.* (*31*) introduced an ankle exoskeleton controller based on a quadratic fit between foot force sensor data and user ankle moments during level walking. This work was extended to incline/decline walking, stair ascent/descent, and even mixed terrain with notable outcomes across able-body and clinical populations (*37*–*39*). Although promising, it remains unclear how this approach would extend to joints beyond the ankle or generalize to additional tasks where the mapping between foot force sensor measurements and joint moments is more complex. Alternatively, energy-shaping methods have been developed for assisting the hip, knee, and ankle during multiple ambulation modes and during sit-stand cycles (*29*, *30*). These approaches have demonstrated impressive offline estimation results and potential benefits in lower-limb muscle activation; however, substantial user benefits and online estimation accuracy relative to ground-truth inverse dynamics have not yet been demonstrated. As such, the development of a unified exoskeleton controller capable of autonomously assisting the user across a wide variety of ambulation modes and intensities has remained an open topic of research—maintaining the divide between in-lab exoskeleton technology and real-world benefits.

[1]George W. Woodruff School of Mechanical Engineering, Georgia Institute of Technology, Atlanta, GA 30332, USA. [2]Institute for Robotics and Intelligent Machines, Georgia Institute of Technology, Atlanta, GA 30332, USA. [3]Department of Brain and Cognitive Sciences, Massachusetts Institute of Technology, Cambridge, MA 02139, USA.
*Corresponding author. Email: dmolinaro3@gatech.edu

In this study, we present an end-to-end framework for controlling a lower-limb robotic exoskeleton based on instantaneous estimates of the user's joint moments using deep learning, deemed unified joint moment control (Movie 1 and Fig. 1). We validated the unified controller using our autonomous hip exoskeleton (figs. S1 and S2) because hip-centric assistance has substantially improved human energetics during several ambulation modes in previous studies (*3*, *7*, *9*, *43*, *44*), likely by offloading the large positive power requirements of the hip joint (*45*) while minimizing any metabolic penalties caused by distal-borne mass (*46*). Computing hip moments from inverse dynamics requires distal joint kinematics (*41*), suggesting the need for complex, cumbersome sensor suites. Instead, we used a temporal convolutional network (TCN) (*47*) to estimate the total hip flexion/extension moments of the user, including both the biological hip moment and the exoskeleton torque, on the basis of kinematic data from embedded exoskeleton sensors (fig. S3). In addition, the structure of the TCN leveraged temporal information in the input data as a substitute for multijoint sensing, resulting in accurate hip moment estimates without any user-specific calibration or other user state information, such as ambulation mode. Thus, when integrated into the exoskeleton controller via a scale, delay, and filter at the mid-level layer (fig. S4), the hip moment estimates enabled the exoskeleton controller to autonomously modulate assistance across a wide range of ambulatory conditions without any manual experimenter or user intervention.

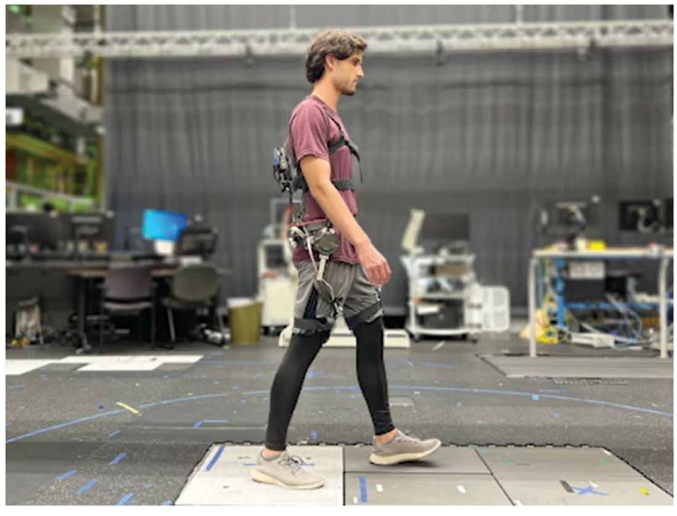

Movie 1. A summary of the results of this study is provided, including representative trials demonstrating the online performance of the unified controller.

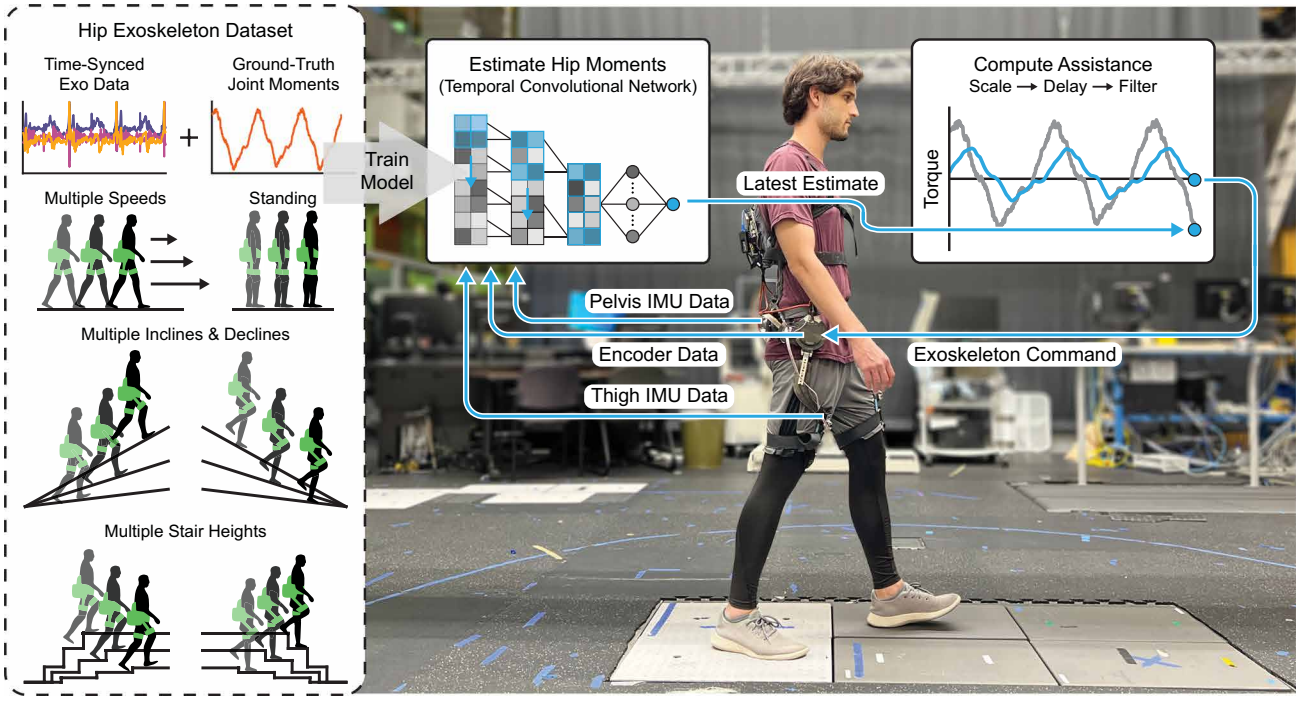

Fig. 1. Unified joint moment control. A photograph of an individual walking with the autonomous, robotic hip exoskeleton is shown. A TCN, trained using time-synced exoskeleton data and ground-truth labels (depicted left of the photograph), used data from the encoders and IMUs mounted on the exoskeleton to estimate the user's hip moments. When implemented on the device, instantaneous hip moment estimates from the TCN were converted to desired exoskeleton assistance using a mid-level control layer, which scaled, delayed, and filtered the estimates. Mid-level scaling provided a percentage of the total estimated moment as assistance, delay increased the positive mechanical work done by the exoskeleton, and filtering smoothed the assistance. By training the hip moment estimator with data from a variety of conditions, the controller seamlessly adapted assistance across different users, ambulation modes, and ambulation intensities without the need for user-specific calibration data.

To validate our approach, we measured user metabolic cost, the rate of whole-body human energy expenditure needed to move, during level-ground walking and 5° ramp ascent, because both demand large amounts of work from the hip joint (*40*, *45*). Given the lightweight design of our exoskeleton and the natural changes in assistance of the unified controller across participants and across modes, we hypothesized that walking with the exoskeleton using the unified controller (Unified Control) would reduce user metabolic cost during both level-ground and incline walking compared with wearing the exoskeleton without assistance (Zero Torque) and compared with walking without the exoskeleton (No Exo) (H1). As an additional benchmark, we also measured user metabolic cost when walking with exoskeleton assistance from previously optimized splines (*20*, *21*) (Spline Control), representing the state of the art in mode-specific, "off-the-shelf" exoskeleton control. To further decompose the energetic effects of our system on the user, we quantified the effect of the unified controller on user lower-limb positive joint work compared with No Exo. We hypothesized that Unified Control would enable users to substitute their hip joint work with that of the exoskeleton (*48*), reducing their lower-limb positive mechanical work compared with No Exo (H2).

In addition, we quantified the accuracy of our deep learning–based hip moment estimator when integrated into the exoskeleton controller (deployed online) during level-ground walking, ramp ascent/descent, and stair ascent/descent under 35 total conditions of varying walking speeds, ground slopes, and stair heights. Further simulating real-world conditions, the TCN was also tested during neutral standing, during transitions between walking and standing, and during conditions that were not included in the training set. We tested the TCN online, because closing the loop between estimator outputs and human-exoskeleton dynamics can lead to error propagation undetected in offline analyses (*49*). We compared our approach with a Baseline method designed to emulate bioinspired exoskeleton controllers from previous studies (*7*, *26*). The Baseline method predicted the average hip moment profile as a function of gait phase, computed a priori from the training set, for each ambulation mode and assumed a perfectly accurate ambulation mode and gait phase oracle (the best-case scenario). Because the TCN should model changes in hip moments across users, across intensities, and across strides, we hypothesized that the TCN estimates would have a lower root mean square error (RMSE) and a higher R^2 with respect to the ground-truth hip moments compared with the Baseline method (H3 and H4, respectively).

Thus, this work presents and validates a unified exoskeleton controller, which leveraged deep learning to accurately map exoskeleton sensor data to user hip moments. The controller autonomously adapted assistance with changes in user joint demand across a wide range of walking speeds, ground slopes, and stair heights without any tuning or experimenter intervention. Using the unified controller, we measured significant improvements in user metabolic cost, relative to No Exo and Zero Torque, and in lower-limb positive joint work, relative to No Exo (Zero Torque was not collected), during level-ground and incline walking. We also found that the TCN significantly outperformed the Baseline method for estimating user hip moments across a variety of conditions. Further, we have released the time-synced time series data of human biomechanics and exoskeleton sensor data used in this study (34 total participants across the four phases of experimental data collections) in conjunction with this publication, increasing the accessibility of machine learning–enabled exoskeleton technology. With these advancements in exoskeleton control and with the corresponding dataset released with this study, exoskeleton technology moves ever closer to being realized in daily life.

RESULTS

Augmenting human metabolic cost during level-ground walking and ramp ascent

User metabolic cost was measured from 10 participants during level-ground walking and 5° ramp ascent under four conditions: Unified Control using a TCN trained from 14 participants of data (from phases 1 and 2 of the experimental protocol), Spline Control, No Exo, and Zero Torque (Fig. 2). The TCN training set included level-ground walking, ramp ascent/descent, stair ascent/descent, standing, and stand-to-walk and walk-to-stand transitions. During level-ground walking, Unified Control significantly reduced metabolic cost by 0.12 ± 0.13 W/kg (5.4 ± 5.6%) compared with No Exo ($P = 0.0219$) and by 0.32 ± 0.07 W/kg (12.7 ± 2.8%) compared with Zero Torque ($P = 6 \times 10^{-8}$), shown in Fig. 2B. Further, during ramp ascent, Unified Control resulted in significant metabolic cost reductions of 0.57 ± 0.24 W/kg (10.3 ± 4.4%) compared with No Exo ($P = 4 \times 10^{-8}$) and of 1.06 ± 0.31 W/kg (17.8 ± 5.1%) compared with Zero Torque ($P = 3 \times 10^{-14}$), shown in Fig. 2E. The unified controller had no significant difference in metabolic cost during level-ground walking compared to Spline Control, with a difference in metabolic cost of less than 0.01 W/kg between the two conditions ($P = 1.0$); however, during ramp ascent, the unified controller significantly reduced metabolic cost by 0.27 ± 0.15 W/kg (5.3 ± 2.8%) compared with Spline Control ($P = 0.0025$).

Reducing joint-level positive mechanical work of the user

To analyze the effect of our controller at the joint level, lower-limb mechanical work was measured across the same 10 participants under the Unified Control and No Exo conditions. The unified controller was deployed using the same hip moment estimator that was used when measuring user metabolic cost. As shown in Fig. 3, the total positive mechanical work of the user's lower-limb joints (sum of hip, knee, and ankle positive work in the sagittal plane) was significantly lower with Unified Control compared with No Exo during both level-ground walking [change of 0.16 ± 0.05 J/kg (17.5 ± 5.7%); $P = 5 \times 10^{-6}$] and ramp ascent [change of 0.16 ± 0.08 J/kg (11.7 ± 6.2%); $P = 2 \times 10^{-4}$]. At the individual joint level, we found that Unified Control significantly reduced the positive mechanical work of the hip joint by 0.12 ± 0.04 J/kg (29.2 ± 10.9%) during level-ground walking ($P = 2 \times 10^{-8}$) and by 0.15 ± 0.08 J/kg (22.8 ± 12.2%) during ramp ascent ($P = 8 \times 10^{-6}$) compared with No Exo (Fig. 3, A and B).

Validating TCN accuracy in the loop

The TCN, when trained from a 24-participant dataset (from phases 1 through 3 of the experimental protocol), was evaluated when implemented in the exoskeleton control loop during 35 conditions, including level-ground walking at speeds ranging from 0.6 to 1.9 m/s, inclines and declines ranging from −15° to 15°, and stairs spanning the range of ADA (Americans with Disabilities Act)–compliant step heights of 10.2 to 17.8 cm (4 to 7 inches) (fig. S5). In addition, the Baseline method served as a comparison with the TCN for hip moment estimation, which predicted hip moments on the basis of the ambulation mode–specific, participant-averaged hip moment profiles from the TCN training set. The Baseline method was

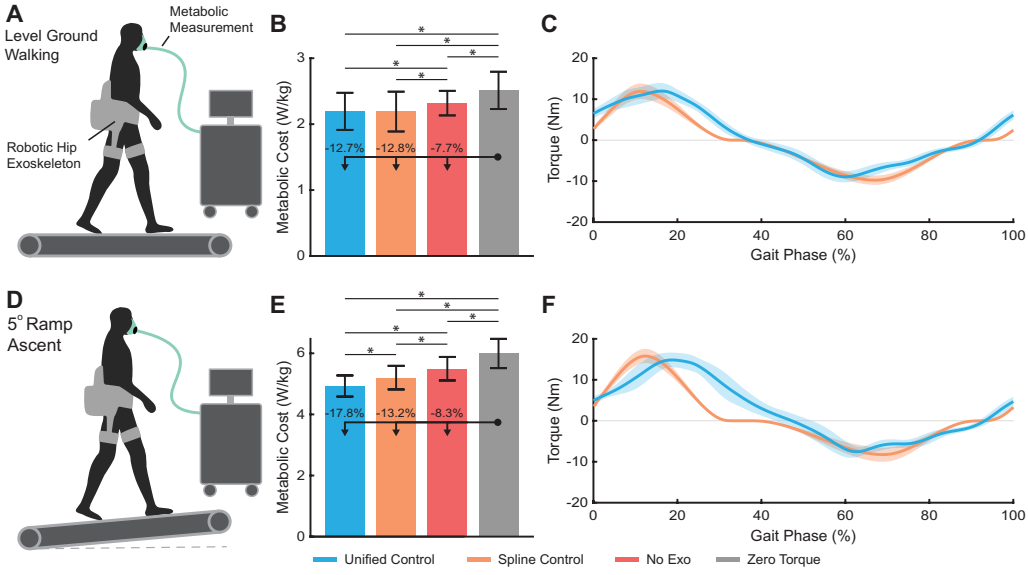

Fig. 2. Exoskeleton effect on user metabolic cost of walking. (**A**) User metabolic cost was measured during level-ground walking at 1.25 m/s while the user wore the exoskeleton with the unified joint moment controller (Unified Control), while the user wore the exoskeleton with a spline-based controller (Spline Control), while the user did not wear the exoskeleton (No Exo), and while the user wore the exoskeleton as it commanded zero torque (Zero Torque). (**B**) The resulting metabolic cost of each condition during level-ground walking is shown, and the percent reduction of each condition relative to Zero Torque is depicted with the arrows. (**C**) The commanded exoskeleton torque averaged across participants is shown for Unified Control and Spline Control during level-ground walking. (**D**) User metabolic cost was also measured during 5° ramp ascent at 1.25 m/s. (**E**) The average metabolic cost resulting from the incline tests is shown. (**F**) The average commanded exoskeleton torques during ramp ascent are shown. Gait cycles were segmented by heel strike, and hip extension is positive. Bars and curves represent means, error bars and shaded regions represent ±1 SD about the mean, and asterisks indicate statistical significance (multiple comparisons, $P < 0.05$, $n = 10$).

Fig. 3. Exoskeleton effect on user lower-limb joint work. The per-stride, positive biological joint work of the hip, knee, ankle, and sum of all three joints (total) during (**A**) level-ground walking and (**B**) 5° ramp ascent is shown. Joint work was measured while participants wore the exoskeleton, which provided assistance using the unified controller (Unified Control), and while participants did not wear the exoskeleton (No Exo). Average power of the exoskeleton and biological hip, knee, and ankle joints is shown during level-ground walking and ramp ascent (**C** to **H**). Gait cycles were segmented by heel strike. All results were computed with respect to the sagittal plane. Bars and curves represent means; error bars and shaded regions represent ±1 SD about the mean. Statistical comparisons of total positive joint work were computed using paired *t* tests, and joint-level comparisons were conducted using multiple comparisons post hoc. Asterisks indicate statistical significance ($P < 0.05$, $n = 10$).

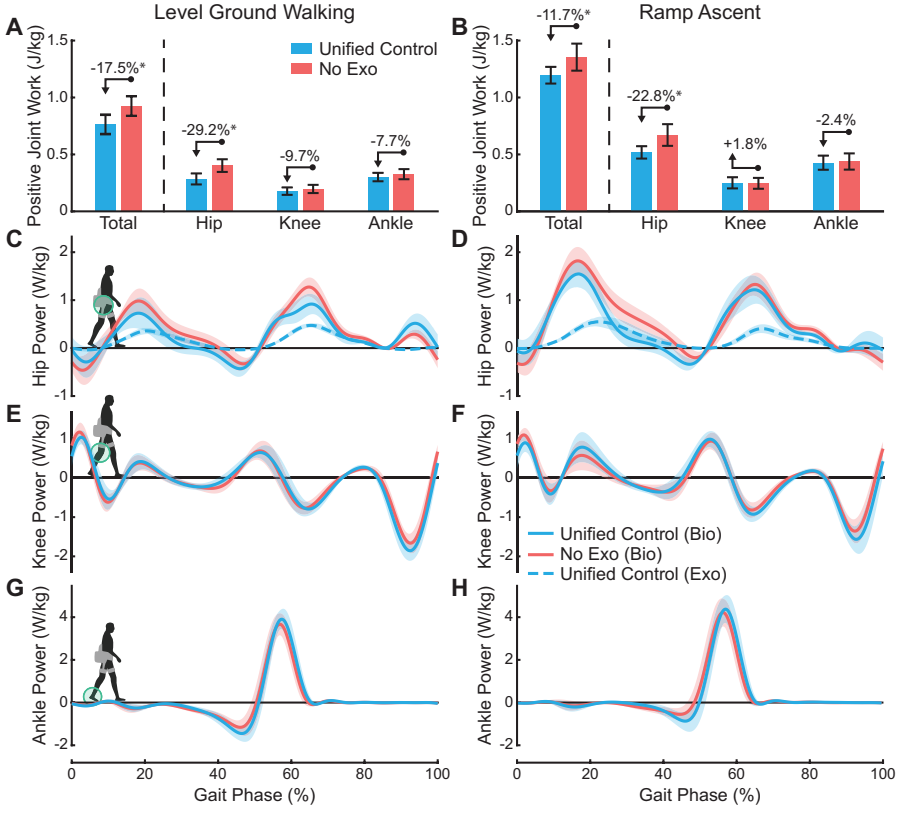

implemented post hoc on the same trials used to evaluate the TCN. The resulting RMSE and R^2 of the TCN and Baseline estimates were computed with respect to the ground-truth hip moments from inverse dynamics.

The overall RMSE of the TCN averaged across the five ambulation modes was 0.142 ± 0.021 N·m/kg, which was significantly lower than the Baseline method [change of 0.035 ± 0.016 N·m/kg (19.8 ± 9.3%); $P = 9 \times 10^{-5}$] (Fig. 4), with representative strides of the TCN estimates shown in Fig. 5. Significant reductions in RMSE within modes were also found for the level-ground [change of 0.060 ± 0.022 N·m/kg (29.1 ± 10.5%); $P = 0.0012$] and ramp descent conditions [change of 0.051 ± 0.035 N·m/kg (27.0 ± 18.8%); $P = 0.0092$]. In addition, the overall R^2 of the TCN was 0.840 ± 0.045, which was significantly higher than that of the Baseline method [change of 0.035 ± 0.034 (4.4 ± 4.2%); $P = 0.0088$] (fig. S6). Further, when comparing the TCN and Baseline methods within ambulation modes, the TCN significantly outperformed the Baseline method in several conditions (Fig. 4C and fig. S6C), often near the extrema within each mode (P values provided in data file S2).

Five of the participants also completed additional trials of neutral standing, stand-to-walk transitions, and walk-to-stand transitions while the unified controller provided assistance on the basis of the TCN estimates. We found that the TCN reduced estimation RMSE during stand-to-walk transitions by 0.081 ± 0.031 N·m/kg (34.9 ± 13.5%) and during walk-to-stand transitions by 0.085 ± 0.014 N·m/kg (35.3 ± 5.7%) compared with the Baseline method (Fig. 4B), with similar improvements in R^2 (fig. S6B). Representative strides during each transition are shown in Fig. 5D. In addition, the estimator naturally turned off assistance during neutral standing, with very little difference in RMSE between the estimates from the TCN and those from the Baseline method, which estimated zero hip moment (Fig. 4B).

To further investigate the real-world viability of our hip moment estimator, we also quantified the effects on TCN performance when each of the 35 ambulatory conditions was included versus excluded from the training set (details provided in Supplementary Methods). In general, the TCN generalized well when tested on previously unseen conditions (fig. S7), with significant differences between hold-in and hold-out RMSE in only 3 of the 35 total conditions. In addition, there were no significant differences in R^2 between hold-in and hold-out conditions.

DISCUSSION

Deep learning–based hip moment estimates yielded autonomous exoskeleton assistance

The unified controller presented in this work autonomously adapted exoskeleton assistance across users, ambulation modes, and ambulation

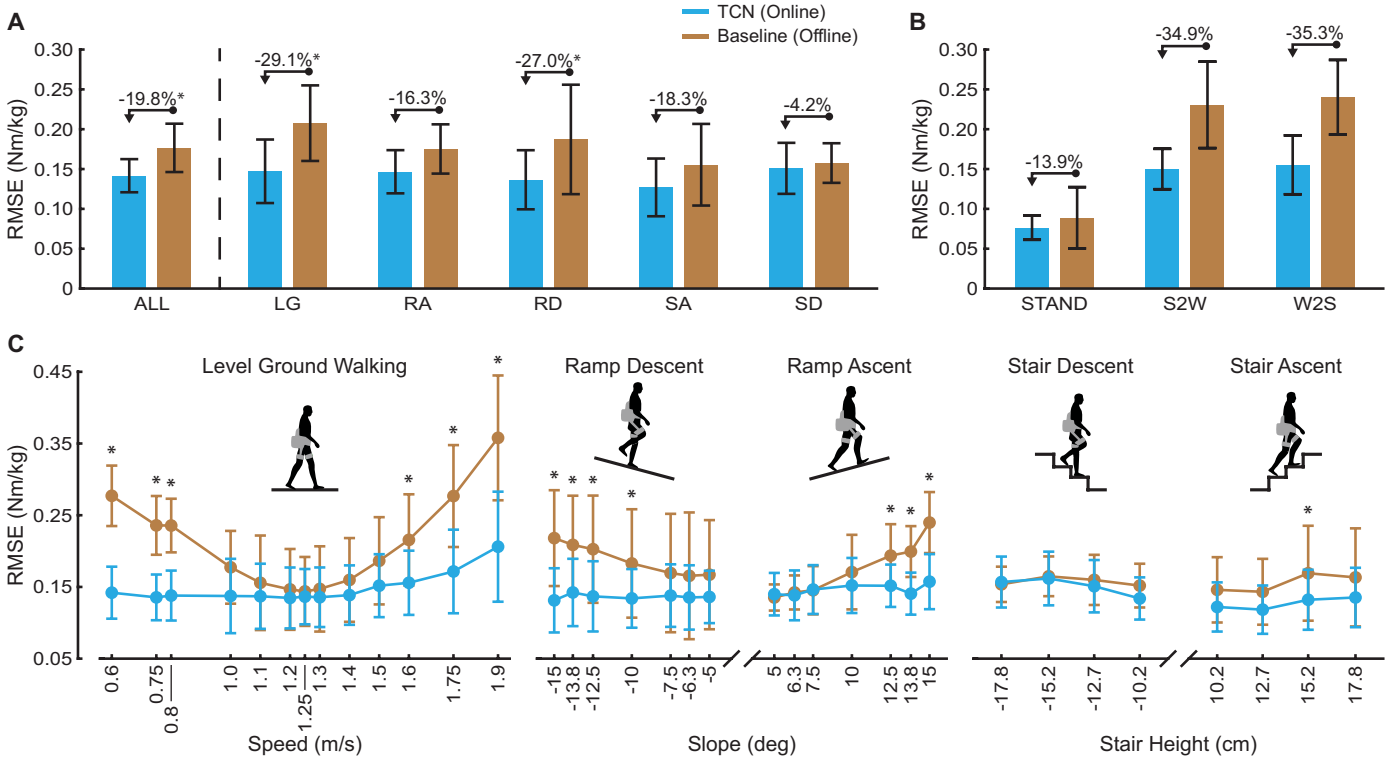

Fig. 4. Hip moment estimation RMSE. (**A**) The average RMSE of the TCN is compared with the RMSE of the Baseline method during level-ground walking (LG), ramp ascent (RA), ramp descent (RD), stair ascent (SA), and stair descent (SD) (multiple comparisons, $n = 10$). The average RMSE across the five ambulation modes (ALL) is also shown (paired t test, $n = 10$). (**B**) The average RMSE of the TCN is shown during neutral standing (STAND), stand-to-walk transitions (S2W), and walk-to-stand transitions (W2S) relative to the Baseline method ($n = 5$, no statistical tests performed). (**C**) The average RMSE of the TCN and Baseline method is shown for each intensity per ambulation mode (multiple comparisons, $n = 10$ for all comparisons except for LG at 1.9 m/s and RD at −15°, which were $n = 9$). All TCN results are based on online estimates used in the control loop. All Baseline results were computed post hoc using the same data. Bars and markers represent means, error bars represent ±1 SD about the mean, and asterisks indicate statistical significance ($P < 0.05$).

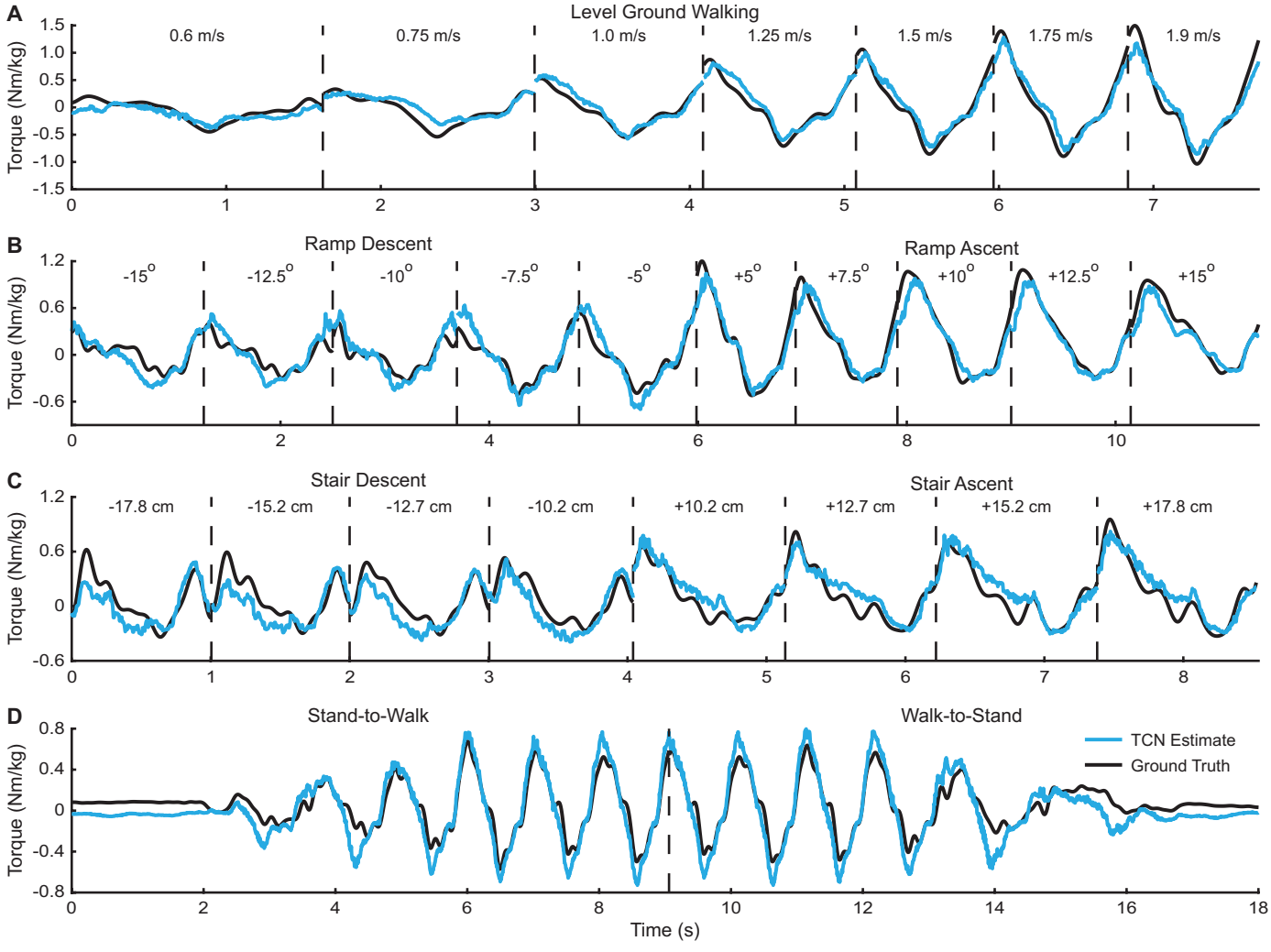

Fig. 5. Representative time series. Examples of hip moments estimated by the TCN and the corresponding ground truth values are shown. (**A**) Representative strides from 7 of the 13 total level-ground walking conditions are shown (average RMSE of the depicted strides is 0.141 N·m/kg). (**B**) Representative strides from 10 of the 14 total inclines and declines are shown (average RSME of the depicted strides is 0.138 N·m/kg). (**C**) Representative strides of stair ascent and descent at each of the tested stair heights are shown (average RMSE of the depicted strides is 0.137 N·m/kg). (**D**) A representative time series of a stand-to-walk and walk-to-stand transition is shown (average RMSE of the depicted strides is 0.128 N·m/kg). The stand-to-walk and walk-to-stand trials were extended from their original segmentation for visual purposes. Within each ambulation mode, the depicted strides are from the same participant. Gait cycles were segmented by heel strike, and hip extension is positive.

intensities without any user-specific calibration data or sensing external to the device. Not only did the deep learning model accurately adapt assistance across all 35 evaluated conditions, but the resulting assistance also provided significant metabolic and joint-level energetic benefits to the user in both ambulation modes evaluated. Specifically, our approach significantly reduced user metabolic cost during both level-ground walking and 5° ramp ascent relative to No Exo and Zero Torque (Fig. 2), confirming hypothesis H1. Although the magnitude of metabolic cost reductions of our controller was similar to those of previous autonomous exoskeleton studies (*3*), modulating assistance across ambulation modes without any experimenter or user intervention overcomes an important barrier when considering exoskeleton technology for real-world deployment. In addition, further iterations of the exoskeleton hardware or optimizations to the mid-level controller could further improve these results compared with No Exo.

Unified control outperformed mode-dependent, off-the-shelf spline control

Previous human-in-the-loop optimization studies have found that the optimized shape of spline-based hip exoskeleton assistance is relatively consistent across users (*20*, *21*). As such, averaging previously optimized torque assistance splines from multiple participants (Spline Control in this study) is an effective exoskeleton control strategy for reducing human effort without additional time-intensive optimization (*50*). Matching metabolic cost reductions compared with Spline Control during level-ground walking demonstrates that the unified controller was as effective as the state of the art for user-independent, mode-specific control but did not require any previous optimization, mode switching, or additional state estimation. During ramp ascent, the unified controller significantly reduced user metabolic cost relative to Spline Control, which was likely a result of the additional 19% of positive mechanical work done by the unified controller compared

with Spline Control, despite scaling the two to have near-equivalent peak torque magnitudes (Fig. 2, C and F). This result was unexpected because we expected Spline Control to be a near-optimal controller (*20*, *21*); however, several considerations may explain this result. First, the splines used in this study were optimized on a different device, with differing torque capabilities and actuator dynamics (*51*); it is possible that human-in-the-loop optimization must be repeated with each new device to maintain energetic benefits. Further, the optimized controller gains from human-in-the-loop optimization may not represent the global optimum, despite often requiring tens of minutes or even hours of walking to converge (*8*, *20*–*22*). Last, the unified controller introduced in this study instantaneously adjusted assistance across participants and across strides, potentially yielding additional benefits compared with the static profiles of Spline Control. Nevertheless, the result of our metabolic tests confirmed that our unified controller both autonomously modulated exoskeleton assistance across modes and generated exoskeleton assistance as beneficial as or better than the previous state of the art in user-independent, off-the-shelf control, a major step toward real-world human augmentation.

Users reduced their joint work to accept exoskeleton assistance

In agreement with our metabolic cost findings and hypothesis H2, the unified controller also significantly reduced the total lower-limb positive mechanical joint work of the user during both level-ground walking and ramp ascent (Fig. 3). We found larger relative reductions in metabolic cost between Unified Control and No Exo during ramp ascent but larger relative reductions in positive lower-limb joint work in level-ground walking. This suggests that the additional benefits in metabolic cost during ramp ascent may come from improved muscle-level efficiencies or reduced cocontraction when wearing the device, hinting that future generations of exoskeleton controllers may benefit even more by accounting for the user's underlying muscle dynamics (*52*).

As expected, the benefits of the unified controller on user lower-limb positive joint work were localized at the hip joint (Fig. 3), with relative reductions of 29.2 and 22.8% relative to No Exo during level-ground walking and ramp ascent, respectively. By delaying the exoskeleton assistance relative to the instantaneous hip moment estimate in the mid-level control layer (Fig. 1 and fig. S4), the unified joint moment controller provided peak assistance torque during the periods of the stride with high hip velocities, increasing the total amount of positive mechanical work provided by the exoskeleton. Thus, the unified controller was able to reduce the positive work at the hip joint by more than 20% despite only scaling the assistance torque to 20% of the total estimated hip moment. This result demonstrates the energetic benefits gained by simply delaying hip exoskeleton assistance relative to the biological joint moment during walking.

Deep learning enabled accurate hip moment estimation in the loop

Overall, the TCN accurately estimated user hip moments across the 35 ambulatory conditions when deployed online (Fig. 4 and fig. S6). Confirming hypotheses H3 and H4, the TCN significantly outperformed the Baseline method in RMSE and R^2, even though the Baseline method in this study assumed a perfectly accurate ambulation mode classifier and gait phase estimator. In practice, mode classifiers and gait phase estimators also incur error (*13*–*17*, *26*–*28*), further increasing the differences between the TCN and Baseline method. Nevertheless, this indicates that the TCN not only captured changes in hip moments as ambulation mode and gait phase varied but also modeled changes in hip moments across participants, across intensities, and/or across strides.

Although multiple studies have investigated wearable sensor–based hip moment estimation offline (*30*, *33*–*36*, *42*), this study provides a rigorous validation with respect to ground-truth inverse dynamics when deployed online. Online validation is critical because closing the loop between model estimates and user biomechanics can greatly reduce model performance. For instance, incorrect ambulation mode estimates can lead to controller instability and further propagate error (*49*). We found that when deployed online, our deep learning–based hip moment estimator obtained similar or even better performance compared with previous offline analyses (*34*–*36*, *42*). For instance, Forner-Cordero *et al.* (*42*) analyzed the effects of replacing force plate measurements with pressure insole estimates when computing inverse dynamics, resulting in a hip moment estimation RMSE of 0.15 N·m/kg and correlation coefficient of 0.92 (approximate R^2 of 0.85) during level-ground walking. For comparison, the TCN in this study resulted in an estimation RMSE of 0.147 ± 0.040 N·m/kg and R^2 of 0.879 ± 0.045 during level-ground walking across all speeds without the need for any external sensors or data, demonstrating the benefits of our data-driven approach. Further, in our previous work, we used data from a hip goniometer and simulated trunk and thigh inertial measurement units (IMUs) to train a TCN for estimating hip moments across level-ground walking, ramp ascent/descent, and stair ascent/descent (*34*). This previous study resulted in an average RMSE of 0.131 N·m/kg and R^2 of 0.88, which was state of the art for offline, participant-independent human hip moment estimation based on wearable sensors. As shown in Fig. 4 and fig. S6, the hip moment estimator in this study maintained similar performance (average online RMSE of 0.142 ± 0.021 N·m/kg and R^2 of 0.840 ± 0.045) despite additional sensor noise from exoskeleton actuation and closed-loop dynamics between hip moment estimates, exoskeleton assistance, and the resulting kinematics of the user. Thus, using a single regression model for high-level state estimation mitigated error propagation from estimator-controller dynamics, increasing overall controller reliability.

The unified controller extended to transient and previously unseen conditions

Transitions between standing and walking are extremely common in community ambulation (*53*) but typically are not accommodated by conventional exoskeleton controllers given the challenge of parameterizing mode transitions. By naturally varying assistance based on the estimated joint moments, the unified joint moment controller seamlessly adjusted exoskeleton assistance through mode transitions, without the need for any additional modifications to the controller (see Fig. 4B and fig. S6B with representative strides in Fig. 5D).This result also aligns with our previous work, which quantified TCN hip moment estimation performance during ambulation mode transitions (*34*), suggesting that the TCN estimates remain viable even during transient ambulation.

Further, the model generalized well when tested on conditions absent from the training set (fig. S7). Model RMSE comparing hold-in versus hold-out conditions was only affected at the extrema of the dataset, meaning that the model interpolated between conditions in the training set well but began to lose performance during extrapolation. We did not find any significant differences in R^2 between holding in and holding out each condition. This suggests that the

TCN maintained the correct "shape" of the hip moments but likely began to improperly scale the magnitudes when extrapolating to high intensities. Nevertheless, this result promotes the need for diverse datasets consisting of large variations in condition and intensity to assist model generalization, which is a key consideration for deploying these systems in the wild.

Human-exoskeleton dataset of multimodal ambulation

To reduce the barrier to entry of machine learning–enabled exoskeleton research, we have released the complete set of exoskeleton and human biomechanical time series data associated with this study. The dataset was collected with 34 total participants, which was large enough to demonstrate diminishing returns in model accuracy improvements with respect to increasing training set size (fig. S8). Further, this dataset could also be used to develop algorithms that eliminate the need for device-specific data when developing data-driven exoskeleton controllers, perhaps by building from our data transformation approach outlined in Supplementary Methods, which would greatly improve the accessibility of this technology.

Limitations

This study had multiple limitations. We added a second onboard processor (the machine learning coprocessor) to run the TCN online, which added mass (5% of total), additional power requirements, and software complexity to the system. In addition, the TCN used a substantial amount of device-specific (although not user-specific) training data. Training the TCN from data collected on a different hip exoskeleton did yield a feasible model for initial controller development (see Supplementary Methods); however, a detailed analysis of transferring data across multiple devices was outside the scope of this study. Another limitation of this study was that the metabolic cost and joint work analyses were conducted using a different model (trained from 14 participants of data) compared with the analysis of online model performance (trained from 24 participants of data). It is possible that further metabolic cost and joint work experiments could yield even better results using the updated hip moment estimator, meaning that our results likely represent a lower bound of what is achievable with the unified controller. In addition, although our unified control framework may generalize to other human degrees of freedom, this study only investigated hip flexion/extension moment estimation and assistance. Last, the accuracy and corresponding user outcomes of the unified controller were only evaluated on able-body participants. Although exoskeleton technology could greatly benefit able-body individuals in many real-world applications, translating this technology to individuals with mobility impairments could also lead to substantial benefits.

Conclusion

In general, this work presents a model-free framework that unifies exoskeleton control across a variety of ambulatory conditions. Where previously proposed unified controllers have used anatomical models calibrated with relatively small amounts of data (*29*–*31*, *37*–*39*), we leveraged deep learning with a large amount of labeled training data. The result was a unified controller that effectively augmented user energetics and could adapt to a very broad range of ambulation modes and intensities. This presents a major advancement in the effort of human augmentation with applicability to a broad range of researchers, technologists, and future end users of exoskeleton technology, many of whom may be one and the same. We expect that this technology will enable researchers to ask new questions about human mobility and augmentation that take place off the treadmill and in more realistic settings. For technologists interested in large-scale health monitoring, for instance, our joint moment estimator could also be used as a wearable sensor–based solution to monitor joint kinetics during daily life. Last, for the end user, we hope that this technology will spur safer and more efficient efforts, including those in factories and warehouses, high-endurance missions like search and rescue, and in athletics and exercise at the professional or recreational level.

MATERIALS AND METHODS

Participants and experimental protocol

This study consisted of four phases, involving the enrollment of 25 able-bodied participants and the use of a nine-participant preexisting dataset from our previous work (*35*). All participant information relevant to this study is provided in table S1, and each participant provided written informed consent according to the protocols approved by the Georgia Institute of Technology Institutional Review Board. To ensure that the hip moment estimator was consistently evaluated on a user-independent basis, meaning trained without user-specific data, each participant only participated in one of the four phases of the study protocol. During each phase, motion capture and ground reaction force (GRF) data were collected (fig. S5), time-synced with the exoskeleton sensor data, and used to compute ground-truth joint moments from OpenSim inverse dynamics (*54*, *55*). A summary of the experimental methods is provided below with a detailed description provided in Supplementary Methods.

The first phase of this study consisted of transforming a nine-participant, preexisting dataset collected using a different hip exoskeleton to be used as TCN training data compatible with our device (*35*). Specifically, the dataset was collected with the same exoskeleton sensor modalities as those of our custom hip exoskeleton but had different IMU placements. When collecting the dataset, each participant walked over level ground, along four inclines and declines with ground slopes ranging from 7.8° to 12.4°, and up and down a staircase at four different stair heights ranging from 10.2 to 17.8 cm. The dataset consisted of exoskeleton sensor data and corresponding ground-truth joint moments. To transform the dataset for use in this study, IMU transforms were computed empirically from a single-participant experiment, which adjusted the positions and orientations of the recorded IMU data to match those of our custom hip exoskeleton. All other protocols and analyses were conducted using our custom hip exoskeleton (fig. S1).

The second phase of this study consisted of collecting device-specific labeled data using our custom hip exoskeleton from five participants. During phase 2, the hip exoskeleton provided assistance using the unified controller, in which the hip moment estimator was trained from the phase 1 dataset. Each participant completed the same trials conducted in phase 1, along with additional standing, stand-to-walk, and walk-to-stand trials.

The third phase of this study was conducted with 10 participants to evaluate the effects of the unified controller on user metabolic cost and lower-limb positive mechanical joint work. The hip moment estimator used throughout phase 3 was trained on the phase 1 and 2 datasets. The phase 3 protocol was subdivided into two sessions. Session 1 served as a training session for walking with the exoskeleton, provided an additional dataset for model training and

evaluation, and served as the session for analyzing user lower-limb mechanical joint work during level-ground walking and 5° ramp ascent with the unified controller (Unified Control) and without wearing the exoskeleton (No Exo). While motion capture and GRF data were recorded, participants walked on a level treadmill at nine speeds ranging from 0.75 to 1.75 m/s, on an inclined/declined treadmill at 10 slopes ranging from −15° to 15°, and up and down a staircase at four stair heights ranging from 10.2 to 17.8 cm using the unified controller. Participants also completed No Exo trials of level walking and 5° ramp ascent at 1.25 m/s, which were used in the joint work analysis.

During session 2 of phase 3, metabolic data were measured during level-ground walking and 5° ramp ascent, both at 1.25 m/s after completing 16 min of habituation. Participants completed the metabolic trials under four conditions using a within-participant counterbalanced design: Unified Control; Spline Control, which provided assistance based on previously optimized level ground and 5° ramp ascent assistance trajectories (*20*, *21*); No Exo; and Zero Torque, which consisted of wearing the exoskeleton while it commanded zero torque.

When evaluating the effects of the training set size on TCN performance, the model continued to improve when adding the phase 3 data (details in Supplementary Methods). Thus, we conducted phase 4 of the experimental protocol, in which 10 additional participants used the unified controller while motion capture and GRF data were collected. During phase 4, the TCN was trained using the data from phases 1, 2, and 3. Participants walked on a level treadmill (13 walking speeds ranging from 0.6 to 1.9 m/s), on an inclined/declined treadmill (14 ground slopes ranging from −15° to 15°), and up and down a staircase (four stair heights ranging from 10.2 to 17.8 cm). To test the hip moment estimator on previously unseen conditions, four level-ground walking speeds and two inclines/declines in this study phase were not collected in any of the previous phases used for training the model. In addition, two of the stair ascent/descent trials were repeated in which each corresponding stair height was withheld from the hip moment estimator training set. Five of the 10 participants also completed trials of neutral standing, stand-to-walk transitions, and walk-to-stand transitions.

Robotic hip exoskeleton

This study used a custom-designed exoskeleton that provided sagittal plane hip torque assistance of up to 18 N·m [~30% of peak biological hip moments during walking (*40*)], shown in fig. S1. The system was fully autonomous, meaning that all components were self-contained. The exoskeleton measured angular position from actuator-mounted encoders in addition to linear acceleration and angular velocity from three IMUs mounted on the exoskeleton backplate and left and right thigh struts. Encoder velocity was also computed online using backward finite differencing and was low-pass filtered with a 10-Hz cutoff frequency. A graphics processing unit–enabled secondary processor mounted onboard the device was used for online TCN deployment. The total exoskeleton mass was 4.8 kg, including electronics and batteries. Additional information is provided in Supplementary Methods and in figs. S1 and S2.

Hip moment estimation using a TCN

We used a TCN (*47*) to estimate the exoskeleton user's hip flexion/extension moments on the basis of measurements from the onboard exoskeleton sensors (fig. S3). TCNs use dilated causal one-dimensional convolution to efficiently map patterns in the input sequence data to the target output (fig. S3C), replacing the need for hand-engineered feature extraction methods (*33*, *56*). In addition, the fixed input sequence length of TCNs has been shown to retain information over longer periods of time than recurrent networks (*47*), suggesting that they can better leverage time history information on larger timescales compared with alternative neural network architectures. As such, TCNs have been successful in many sequence modeling tasks (*34*, *47*, *57*), including achieving state-of-the-art offline performance in human hip moment estimation compared with alternative deep learning models, which we demonstrated in our previous work (*34*, *35*).

The TCN used for hip moment estimation in this study was implemented as described by Bai *et al.* (*47*) using the hyperparameters optimized in our previous work (*34*). The input sequence of the TCN consisted of the ipsilateral actuator encoder position and velocity, six-axis ipsilateral thigh–mounted IMU data, and six-axis pelvis-mounted IMU data. Sensor data from the contralateral limb were not included as input to the model because the majority of the training and testing conditions included symmetric movements, which could cause the model to overfit to this type of behavior. On the basis of the selected hyperparameters of the model, the input sequence to the TCN was composed of a $\mathbb{R}^{180\times14}$ $\mathrm{R}^{187\times14}$ sequence consisting of the latest 930 ms of exoskeleton sensor data. Given an input sequence, the model estimated the instantaneous flexion/extension moment of the user's left or right hip, scaled by the participant's body mass. Ground-truth hip moments from our biomechanical model, which were used as the labels during model training, were the sum of both the biological hip moment and the exoskeleton torque (the total hip flexion/extension moment at the joint). This means that the TCN was trained to estimate the total hip moment, which helped to preserve the mapping between the kinematic input data and resulting joint moments across variations in exoskeleton assistance. Additional information about the TCN hyperparameters, implementation, and training is provided in Supplementary Methods.

Exoskeleton mid-level control

Because hip exoskeleton assistance that solely mimics the user's biological hip moments is likely suboptimal for augmenting human energetics (*20*, *21*, *58*), we designed a three-step mid-level control layer to convert hip moment estimates into exoskeleton assistance (fig. S4). First, the incoming hip moment estimates were scaled by 20% of their total magnitude. This assistance magnitude has previously been shown to benefit the user (*59*) and resulted in peak torque assistance close to the maximum assistance the exoskeleton could provide. The estimated hip moments were then delayed using a first-in-first-out buffer before being used to command the exoskeleton (see details below). Last, the delayed torque values were low-pass filtered using a second-order Butterworth filter with a 10-Hz cutoff frequency to smooth the commanded torque, imparting an additional 25 ms of delay to the signal.

Delaying peak hip assistance timing relative to the biological hip moment can provide additional metabolic benefits to the user (*20*, *58*). As Ding *et al.* (*58*) explained, delayed hip assistance increases the amount of positive mechanical work done by the exoskeleton because the peak assistance of a delayed controller better aligns with peak hip velocities during the stride. Using the data available from Camargo *et al.* (*40*), we found that delaying exoskeleton assistance by 125 ms relative to the biological hip moment could theoretically

increase the positive mechanical work done by the exoskeleton during level walking by 70% (fig. S4A). In support of this delayed assistance strategy, we found that delaying exoskeleton assistance between 100 and 150 ms was preferred by several novice and expert users during pilot testing compared with smaller delay magnitudes; however, in an $N = 3$ pilot study (detailed in Supplementary Methods), user metabolic cost was not sensitive to delay magnitudes ranging from 75 to 175 ms (fig. S4B). Specifically, the mid-level control delays that we tested only affected user metabolic cost by a maximum of 2.9% across level-ground walking and 5° ramp ascent. Testing even smaller delays may result in larger metabolic penalties, especially given that the 75-ms condition was the worst metabolically; however, these small delays were omitted from the pilot study because they were uncomfortable to the user. In addition, delays below 35 ms could not be tested because of controller limitations from filter delay and worst-case model inference latency. For the remainder of this study, a programmed delay of 100 ms (total delay of 125 ms including the low-pass filter) was used to minimize overall delay and to align with user preference.

Analyzing online hip moment estimation accuracy

The estimated hip moments recorded onboard the exoskeleton during phase 4 of the experimental protocol were aligned in time with the ground-truth hip moments post hoc to evaluate the accuracy of the TCN when integrated into the unified controller. Two common performance metrics were used to analyze the estimator accuracy (*30*, *31*, *34*, *42*): the interparticipant average RSME and the interparticipant average of the square of the Pearson correlation coefficient (R^2). Average RMSE provided an absolute metric of error and is easily compared to previous studies that have investigated wearable sensor–based joint moment estimators. Average R^2 provided a nondimensional metric to analyze the goodness of fit of the TCN, meaning the amount of variance in the ground-truth hip moments explained by the TCN estimates via a fitted line. When considering joint moment estimation for exoskeleton control, R^2 also provided a metric for analyzing the ability of the model to correctly estimate the shape of the hip moment signal, ignoring error induced from incorrect scaling or bias. In general, this provided a useful metric to evaluate the utility of the hip moment estimator given that scale and bias of the signal could be modified on the fly by the mid-level exoskeleton control layer as needed.

Results reported per intensity, as in per walking speed, ground slope, and stair height, were individually computed per condition and then averaged across participants. Results reported per ambulation mode were computed by taking the average of the results computed per intensity within the respective mode, for instance, the average of the RMSE values computed per level-ground walking speed then averaged across participants. Overall results were computed similarly by averaging the results computed per ambulation mode, then averaging across participants.

The accuracy of the TCN was benchmarked against a Baseline method designed to emulate conventional exoskeleton controllers that use predefined ambulation mode–specific curves to compute assistance on the basis of gait phase estimates (*7*, *26*, *43*). Specifically, the Baseline method was implemented post hoc and estimated the user's hip moments on the basis of a precomputed hip moment curve for each ambulation mode. The hip moment curve for each ambulation mode (level-ground walking, ramp ascent, ramp descent, stair ascent, and stair descent) was computed as the interparticipant average hip moment over the stride from the ground-truth hip moments in the same dataset used to train the TCN in phase 4 (the hip moment data from phases 1, 2, and 3 of the study protocol). During stand-to-walk and walk-to-stand transitions, the Baseline method used the level-ground walking profile. In addition, the Baseline method simply predicted zero hip moment for the standing trials. In all cases, the Baseline method was given access to a perfectly accurate ambulation mode classifier and gait phase estimator that has error in practice (*9*, *13*–*16*, *26*, *27*), meaning that our benchmark represented the best-case (yet unrealistic) scenario for estimating hip moments from mode-specific curves. In this case, outperforming the Baseline method meant that the participant-independent TCN captured interparticipant, intercondition, and/or interstride variability that the Baseline method could not represent.

Statistical analyses

All statistical tests were conducted using Minitab v19 with an α level of significance of 0.05. Further, all statistical tests were computed using repeated-measures (within-participant) methods. When comparing differences among multiple factors and/or multiple within-factor conditions, a post hoc multiple comparisons test was used to identify significant pairwise differences in the case that significant effects were found from an analysis of variance (ANOVA). All post hoc multiple comparisons were conducted using a Bonferroni correction to control the family-wise error rate. The Bonferroni correction can greatly reduce the statistical power of each pairwise comparison when many pairwise matches exist. In addition, many of the possible pairwise comparisons within each analysis were irrelevant to our hypotheses. Thus, we only evaluated a subset of the possible pairwise comparisons, which were selected a priori (before looking at the results) to limit the amount that each P value needed to be adjusted. Because Minitab did not support this planned comparison approach, we ran a full multiple comparisons test after each ANOVA that yielded statistical significance and adjusted the P values to account for the reduced number of comparisons being evaluated. Metabolic cost comparisons across the four tested exoskeleton assistance conditions (Unified Control, Spline Control, No Exo, and Zero Torque) were analyzed for a main effect using a one-way ANOVA followed by a multiple comparisons test. Differences in positive joint work between the exoskeleton conditions (Unified Control and No Exo) across the lower-limb joints (hip, knee, and ankle) were evaluated using a two-way ANOVA for level ground and ramp ascent. Pairwise comparisons were only conducted for testing significant differences between Unified Control and No Exo within each joint. In addition, the total positive lower-limb joint work resulting from Unified Control and No Exo were compared separately from the other joints using a paired t test for each ambulation mode.

The same statistical tests were run for analyzing both the RMSE and the R^2 of the hip moment estimates from the TCN and Baseline method. The overall average results of the TCN across the level-ground, ramp ascent, ramp descent, stair ascent, and stair descent conditions were compared with those of the Baseline method using a paired t test. For comparisons at the ambulation mode level, a two-way ANOVA was used to test for significant main and interaction effects across ambulation modes and between estimators (the TCN and Baseline method). A post hoc multiple comparisons test was also used to test for pairwise differences between the two estimators during each ambulation mode. Within each ambulation mode, a

two-way ANOVA was used to test for significant main and interaction effects across ambulation mode intensity and between estimators. In addition, a post hoc multiple comparisons test was used to test for significant differences between the TCN and Baseline method within each intensity.

Supplementary Materials

This PDF file includes:
Methods
Figs. S1 to S8
Tables S1 to S3
References (*60*–*66*)

Other Supplementary Material for this manuscript includes the following:
Data files S1 and S2
MDAR Reproducibility Checklist

REFERENCES AND NOTES

1. R. Bogue, Robotic exoskeletons: a review of recent progress. *Indust. Robot: An Intl J.* **42**, 5–10 (2015).
2. G. K. Ela, Epidemiology of wilderness search and rescue in New Hampshire, 1999–2001. *Wilderness Environ. Med.* **15**, 11–17 (2004).
3. G. S. Sawicki, O. N. Beck, I. Kang, A. J. Young, The exoskeleton expansion: improving walking and running economy. *J. Neuroeng. Rehabil.* **17**, 1–9 (2020).
4. C. Siviy, L. M. Baker, B. T. Quinlivan, F. Porciuncula, K. Swaminathan, L. N. Awad, C. J. Walsh, Opportunities and challenges in the development of exoskeletons for locomotor assistance. *Nat. Biomed. Eng.* **4**, 456–472 (2022).
5. P. Malcolm, W. Derave, S. Galle, D. De Clercq, A simple exoskeleton that assists plantarflexion can reduce the metabolic cost of human walking. *PLOS ONE* **8**, e56137 (2013).
6. L. M. Mooney, E. J. Rouse, H. M. Herr, Autonomous exoskeleton reduces metabolic cost of human walking. *J. Neuroeng. Rehabil.* **11**, 151 (2014).
7. K. Seo, J. Lee, Y. Lee, T. Ha, Y. Shim, Fully autonomous hip exoskeleton saves metabolic cost of walking, in *2016 IEEE International Conference on Robotics and Automation (ICRA)* (IEEE, 2016), pp. 4628–4635.
8. J. Zhang, P. Fiers, K. A. Witte, R. W. Jackson, K. L. Poggensee, C. G. Atkeson, S. H. Collins, Human-in-the-loop optimization of exoskeleton assistance during walking. *Science* **356**, 1280–1284 (2017).
9. J. Kim, G. Lee, R. Heimgartner, D. A. Revi, N. Karavas, D. Nathanson, I. Galiana, A. Eckert-Erdheim, P. Murphy, D. Perry, Reducing the metabolic rate of walking and running with a versatile, portable exosuit. *Science* **365**, 668–672 (2019).
10. T. Yan, M. Cempini, C. M. Oddo, N. Vitiello, Review of assistive strategies in powered lower-limb orthoses and exoskeletons. *Robot. Auton. Syst.* **64**, 120–136 (2015).
11. A. J. Young, D. P. Ferris, State of the art and future directions for lower limb robotic exoskeletons. *IEEE Trans. Neural Syst. Rehabil. Eng.* **25**, 171–182 (2016).
12. M. R. Tucker, J. Olivier, A. Pagel, H. Bleuler, M. Bouri, O. Lambercy, J. del R Millán, R. Riener, H. Vallery, R. Gassert, Control strategies for active lower extremity prosthetics and orthotics: a review. *J. Neuroeng. Rehabil.* **12**, 1 (2015).
13. B. Laschowski, W. McNally, A. Wong, J. McPhee, Environment classification for robotic leg prostheses and exoskeletons using deep convolutional neural networks. *Front. Neurorobot.* **15**, 730965 (2022).
14. I. Kang, D. D. Molinaro, G. Choi, J. Camargo, A. J. Young, Subject-independent continuous locomotion mode classification for robotic hip exoskeleton applications. *IEEE Trans. Biomed. Eng.* **69**, 3234–3242 (2022).
15. J. Camargo, W. Flanagan, N. Csomay-Shanklin, B. Kanwar, A. Young, A machine learning strategy for locomotion classification and parameter estimation using fusion of wearable sensors. *IEEE Trans. Biomed. Eng.* **68**, 1569–1578 (2021).
16. Y. Qian, Y. Wang, C. Chen, J. Xiong, Y. Leng, H. Yu, C. Fu, Predictive locomotion mode recognition and accurate gait phase estimation for hip exoskeleton on various terrains. *IEEE Robot. Autom. Lett.* **7**, 6439–6446 (2022).
17. Y. D. Li, E. T. Hsiao-Wecksler, Gait mode recognition and control for a portable-powered ankle-foot orthosis, in *2013 IEEE 13th International Conference on Rehabilitation Robotics (ICORR)* (IEEE, 2013), pp. 1–8.
18. D. Lee, I. Kang, D. D. Molinaro, A. Yu, A. J. Young, Real-Time User-Independent Slope Prediction Using Deep Learning for Modulation of Robotic Knee Exoskeleton Assistance. *IEEE Robot. Autom. Lett.* **6**, 3995–4000 (2021).
19. R. L. Medrano, G. C. Thomas, C. G. Keais, E. J. Rouse, R. D. Gregg, Real-time gait phase and task estimation for controlling a powered ankle exoskeleton on extremely uneven terrain. *IEEE Trans. Robot.* **39**, 2170–2182 (2023).
20. P. W. Franks, G. M. Bryan, R. M. Martin, R. Reyes, A. C. Lakmazaheri, S. H. Collins, Comparing optimized exoskeleton assistance of the hip, knee, and ankle in single and multi-joint configurations. *Wearable Technol.* **2**, e16 (2021).
21. P. W. Franks, G. M. Bryan, R. Reyes, M. P. O'Donovan, K. N. Gregorczyk, S. H. Collins, The effects of incline level on optimized lower-limb exoskeleton assistance: A case series. *IEEE Trans. Neural Syst. Rehabil. Eng.* **30**, 2494–2505 (2022).
22. Y. Ding, M. Kim, S. Kuindersma, C. J. Walsh, Human-in-the-loop optimization of hip assistance with a soft exosuit during walking. *Sci. Robot.* **3**, eaar5438 (2018).
23. P. Slade, R. Troutman, M. J. Kochenderfer, S. H. Collins, S. L. Delp, Rapid energy expenditure estimation for ankle assisted and inclined loaded walking. *J. Neuroeng. Rehabil.* **16**, 67 (2019).
24. P. Slade, M. J. Kochenderfer, S. L. Delp, S. H. Collins, Personalizing exoskeleton assistance while walking in the real world. *Nature* **610**, 277–282 (2022).
25. Q. Li, M. Young, V. Naing, J. M. Donelan, Walking speed and slope estimation using shank-mounted inertial measurement units, in *2009 IEEE International Conference on Rehabilitation Robotics* (IEEE, 2009), pp. 839–844.
26. I. Kang, D. D. Molinaro, S. Duggal, Y. Chen, P. Kunapuli, A. J. Young, Real-Time Gait Phase Estimation for Robotic Hip Exoskeleton Control During Multimodal Locomotion. *IEEE Robot. Autom. Lett.* **6**, 3491–3497 (2021).
27. M. K. Shepherd, D. D. Molinaro, G. S. Sawicki, A. J. Young, Deep Learning Enables Exoboot Control to Augment Variable-Speed Walking. *IEEE Robot. Autom. Lett.* **7**, 3571–3577 (2022).
28. D. Y. Li, A. Becker, K. A. Shorter, T. Bretl, E. T. Hsiao-Wecksler, Estimating system state during human walking with a powered ankle-foot orthosis. *IEEE/ASME Trans. Mechatron.* **16**, 835–844 (2011).
29. J. Lin, N. V. Divekar, G. C. Thomas, R. D. Gregg, Optimally biomimetic passivity-based control of a lower-limb exoskeleton over the primary activities of daily life. *IEEE Open J. Control Syst.* **1**, 15–28 (2022).
30. J. Zhang, J. Lin, V. Peddinti, R. D. Gregg, Optimal energy shaping control for a backdrivable hip exoskeleton. arXiv:2210.03777 [cs.RO] (7 October 2022).
31. G. M. Gasparri, J. Luque, Z. F. Lerner, Proportional joint-moment control for instantaneously adaptive ankle exoskeleton assistance. *IEEE Trans. Neural Syst. Rehabil. Eng.* **27**, 751–759 (2019).
32. K. G. Rabe, T. Lenzi, N. P. Fey, Performance of sonomyographic and electromyographic sensing for continuous estimation of joint torque during ambulation on multiple terrains. *IEEE Trans. Neural Syst. Rehabil. Eng.* **29**, 2635–2644 (2021).
33. J. Camargo, D. Molinaro, A. Young, Predicting biological joint moment during multiple ambulation tasks. *J. Biomech.* **134**, 111020 (2022).
34. D. D. Molinaro, I. Kang, J. Camargo, M. C. Gombolay, A. J. Young, Subject-Independent, Biological Hip Moment Estimation during Multimodal Overground Ambulation using Deep Learning. *IEEE Trans. Med. Robot. Bion.* **4**, 219–229 (2022).
35. D. D. Molinaro, E. O. Park, A. J. Young, Anticipation and delayed estimation of sagittal plane human hip moments using deep learning and a robotic hip exoskeleton, in *2023 IEEE International Conference on Robotics and Automation (ICRA)* (IEEE, 2023), pp. 12679–12685.
36. E. Dorschky, M. Nitschke, C. F. Martindale, A. J. van den Bogert, A. D. Koelewijn, B. M. Eskofier, CNN-Based Estimation of Sagittal Plane Walking and Running Biomechanics From Measured and Simulated Inertial Sensor Data. *Front. Bioeng. Biotechnol.* **8**, 604 (2020).
37. Y. Fang, G. Orekhov, Z. F. Lerner, Improving the energy cost of incline walking and stair ascent with ankle exoskeleton assistance in cerebral palsy. *IEEE Trans. Biomed. Eng.* **69**, 2143–2152 (2022).
38. S. S. P. A. Bishe, T. Nguyen, Y. Fang, Z. F. Lerner, Adaptive ankle exoskeleton control: Validation across diverse walking conditions. *IEEE Trans. Med. Robot. Bion.* **3**, 801–812 (2021).
39. E. A. Tagoe, Y. Fang, J. R. Williams, Z. F. Lerner, Walking on Real-world Terrain with an Ankle Exoskeleton in Cerebral Palsy. *IEEE Trans. Med. Robot. Bion.* **6**, 202–212 (2023).
40. J. Camargo, A. Ramanathan, W. Flanagan, A. Young, A comprehensive, open-source dataset of lower limb biomechanics in multiple conditions of stairs, ramps, and level-ground ambulation and transitions. *J. Biomech.* **119**, 110320 (2021).
41. D. A. Winter, *Biomechanics and Motor Control of Human Movement* (John Wiley & Sons, 2009).
42. A. Forner-Cordero, H. J. F. M. Koopman, F. C. T. van der Helm, Inverse dynamics calculations during gait with restricted ground reaction force information from pressure insoles. *Gait Posture* **23**, 189–199 (2006).
43. K. Seo, J. Lee, Y. J. Park, Autonomous hip exoskeleton saves metabolic cost of walking uphill, in *2017 International Conference on Rehabilitation Robotics (ICORR)* (IEEE, 2017), pp. 246–251.
44. D.-S. Kim, H.-J. Lee, S.-H. Lee, W. H. Chang, J. Jang, B.-O. Choi, G.-H. Ryu, Y.-H. Kim, A wearable hip-assist robot reduces the cardiopulmonary metabolic energy expenditure during stair ascent in elderly adults: a pilot cross-sectional study. *BMC Geriatr.* **18**, 1–8 (2018).

45. R. W. Nuckols, K. Z. Takahashi, D. J. Farris, S. Mizrachi, R. Riemer, G. S. Sawicki, Mechanics of walking and running up and downhill: A joint-level perspective to guide design of lower-limb exoskeletons. *PLOS ONE* **15**, e0231996 (2020).
46. R. C. Browning, J. R. Modica, R. Kram, A. Goswami, The effects of adding mass to the legs on the energetics and biomechanics of walking. *Med. Sci. Sports Exerc.* **39**, 515–525 (2007).
47. S. Bai, J. Z. Kolter, V. Koltun, An empirical evaluation of generic convolutional and recurrent networks for sequence modeling. arXiv:1803.01271 [cs.LG] (4 March 2018).
48. C. L. Lewis, D. P. Ferris, Invariant hip moment pattern while walking with a robotic hip exoskeleton. *J. Biomech.* **44**, 789–793 (2011).
49. L. J. Hargrove, A. J. Young, A. M. Simon, N. P. Fey, R. D. Lipschutz, S. B. Finucane, E. G. Halsne, K. A. Ingraham, T. A. Kuiken, Intuitive control of a powered prosthetic leg during ambulation: a randomized clinical trial. *JAMA* **313**, 2244–2252 (2015).
50. K. L. Poggensee, S. H. Collins, How adaptation, training, and customization contribute to benefits from exoskeleton assistance. *Sci. Robot.* **6**, eabf1078 (2021).
51. G. M. Bryan, P. W. Franks, S. C. Klein, R. J. Peuchen, S. H. Collins, A hip–knee–ankle exoskeleton emulator for studying gait assistance. *Intl. J. Robot. Res.* **40**, 722–746 (2021).
52. O. N. Beck, L. K. Punith, R. W. Nuckols, G. S. Sawicki, Exoskeletons Improve Locomotion Economy by Reducing Active Muscle Volume. *Exerc. Sport Sci. Rev.* **47**, 237–245 (2019).
53. M. S. Orendurff, J. A. Schoen, G. C. Bernatz, A. D. Segal, G. K. Klute, How humans walk: bout duration, steps per bout, and rest duration. *J. Rehabil. Res. Dev.* **45**, 1077–1090 (2008).
54. S. L. Delp, F. C. Anderson, A. S. Arnold, P. Loan, A. Habib, C. T. John, E. Guendelman, D. G. Thelen, OpenSim: open-source software to create and analyze dynamic simulations of movement. *IEEE Trans. Biomed. Eng.* **54**, 1940–1950 (2007).
55. A. Seth, J. L. Hicks, T. K. Uchida, A. Habib, C. L. Dembia, J. J. Dunne, C. F. Ong, M. S. DeMers, A. Rajagopal, M. Millard, OpenSim: Simulating musculoskeletal dynamics and neuromuscular control to study human and animal movement. *PLoS Comput. Biol.* **14**, e1006223 (2018).
56. H. A. Varol, F. Sup, M. Goldfarb, Multiclass Real-Time Intent Recognition of a Powered Lower Limb Prosthesis. *IEEE Trans. Biomed. Eng.* **57**, 542–551 (2010).
57. A. van den Oord, S. Dieleman, H. Zen, K. Simonyan, O. Vinyals, A. Graves, N. Kalchbrenner, A. Senior, K. Kavukcuoglu, Wavenet: A generative model for raw audio. arXiv:1609.03499 [cs.SD] (12 September 2016).
58. Y. Ding, F. A. Panizzolo, C. Siviy, P. Malcolm, I. Galiana, K. G. Holt, C. J. Walsh, Effect of timing of hip extension assistance during loaded walking with a soft exosuit. *J. Neuroeng. Rehabil.* **13**, 87 (2016).
59. I. Kang, H. Hsu, A. Young, The effect of hip assistance levels on human energetic cost using robotic hip exoskeletons. *IEEE Robot. Autom. Lett.* **4**, 430–437 (2019).
60. J. C. Selinger, J. M. Donelan, Estimating instantaneous energetic cost during non-steady-state gait. *J. Appl. Physiol.* **117**, 1406–1415 (2014).
61. G. Lv, H. Zhu, R. D. Gregg, On the design and control of highly backdrivable lower-limb exoskeletons: A discussion of past and ongoing work. *IEEE Control Syst. Mag.* **38**, 88–113 (2018).
62. M. Grimmer, A. Seyfarth, Mimicking human-like leg function in prosthetic limbs, in *Neuro-Robotics: From Brain Machine Interfaces to Rehabilitation Robotics*, P. Artemiadis, Ed. (Springer, 2014), pp. 105–155.
63. K. He, X. Zhang, S. Ren, J. Sun, Deep residual learning for image recognition, in *Proceedings of the IEEE Conference on Computer Vision and Pattern Recognition* (IEEE, 2016), pp. 770–778.
64. R. W. Nuckols, K. Z. Takahashi, D. J. Farris, S. Mizrachi, R. Riemer, G. S. Sawicki, Mechanics and energetics of walking and running up and downhill: A joint-level perspective to guide design of lower-limb exoskeletons. bioRxiv 2020.04.07.029579 [Preprint]. 7 April 2020. https://doi.org/10.1101/2020.04.07.029579.
65. J. M. Brockway, Derivation of formulae used to calculate energy expenditure in man. *Hum. Nutr. Clin. Nutr.* **41**, 463–471 (1987).
66. U. H. Lee, C.-W. Pan, E. J. Rouse, Empirical characterization of a high-performance exterior-rotor type brushless DC motor and drive, in *2019 IEEE/RSJ International Conference on Intelligent Robots and Systems (IROS)* (IEEE, 2019), pp. 8018–8025.

Acknowledgments: We thank D. Park for help with the overall development of the hip exoskeleton and for assisting with experimental data collection; K. R. Herrin for help developing the human-exoskeleton interface; D. Lee and A. Yu for help developing the custom exoskeleton electronics; G. Choi, J. Jin, and E. O. Park for help with data collection; K. L. Scherpereel and J. K. Leestma for editorial advice; and M. C. Gombolay for advice during the conceptualization of the hip moment estimator and controller framework. **Funding:** This work was supported by National Science Foundation grants 1830215 and 2233164 (A.J.Y.) and National Science Foundation Graduate Research Fellowship Program grant DGE-2039655 (D.D.M.). **Author contributions:** Conceptualization: D.D.M., I.K., and A.J.Y. Methodology: D.D.M., I.K., and A.J.Y. Software: D.D.M. and I.K. Validation: D.D.M. Formal analysis: D.D.M. Investigation: D.D.M. and I.K. Resources: A.J.Y. Data curation: D.D.M. Visualization: D.D.M. and I.K. Funding acquisition: D.D.M. and A.J.Y. Project administration: D.D.M. and A.J.Y. Supervision: D.D.M., I.K., and A.J.Y. Writing—original draft: D.D.M. Writing—review and editing: D.D.M., I.K., and A.J.Y. **Competing interests:** D.D.M., I.K., and A.J.Y. are inventors on a patent (US 18/340,981) filed with the U.S. Patent Office by the Georgia Institute of Technology, which describes some of the state estimation strategies and exoskeleton hardware used in this study. **Data and materials availability:** All data needed to evaluate the conclusions in the paper are present in the paper or the Supplementary Materials. The 34-participant dataset of time-synced exoskeleton data and human biomechanics have been deposited in database https://doi.org/10.5061/dryad.8kprr4xsv.

Submitted 23 May 2023
Accepted 20 February 2024
Published 20 March 2024
10.1126/scirobotics.adi8852